Chapter 4

On-board Power Processor having Inherent V2V Operation with Reduced Components

4.1 Introduction

This chapter presents an on-board power processor having inherent V2V Operation with reduced components. The on-board power processor provides single-phase onboard charging, motoring, vehicle-to-vehicle charging operation, and multiple supplies for EV auxiliaries. All these operations are accomplished by 14 switches, of which three are used to select the function. Further, during V2V charging, six active switches are used for the energy exchange. It improves the efficiency and durability of the proposed multifunction power converter. Conventionally, different converters are used for different functions. It can be understood by the block diagram of that conventional system, as shown in Fig.4. 1.

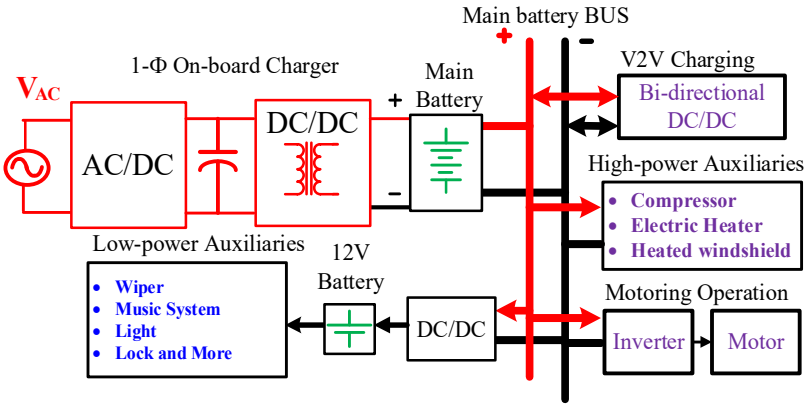

Fig.4. 1 Conventional EV operations by different power converters with an additional 12 V battery.

The following challenges are observed in similar prior works:

1. The integration of prior works involves the integration of only two to three functionalities.
2. An additional 12 V battery and charger are required to power the low-power auxiliaries in EVs [109], [110], [111].
3. During the V2V charging operation, eight switches are used for the energy exchange.
4. In low-power EVs such as Mahindra e2o and GEM e4, the main battery operates at 48 V, which also powers the high-power auxiliaries in EVs. The current demand tends to be significantly higher than high-power EVs such as the Mahindra XUV400, where the main battery voltage is more than 370 V.

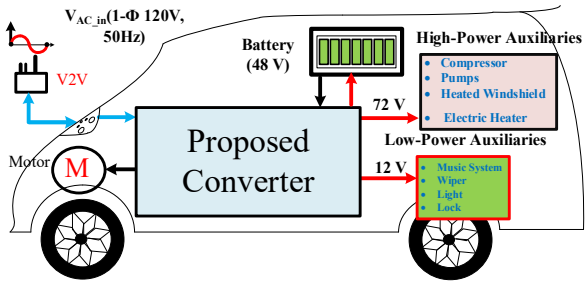

Fig.4. 2 Block diagram of the proposed converter.

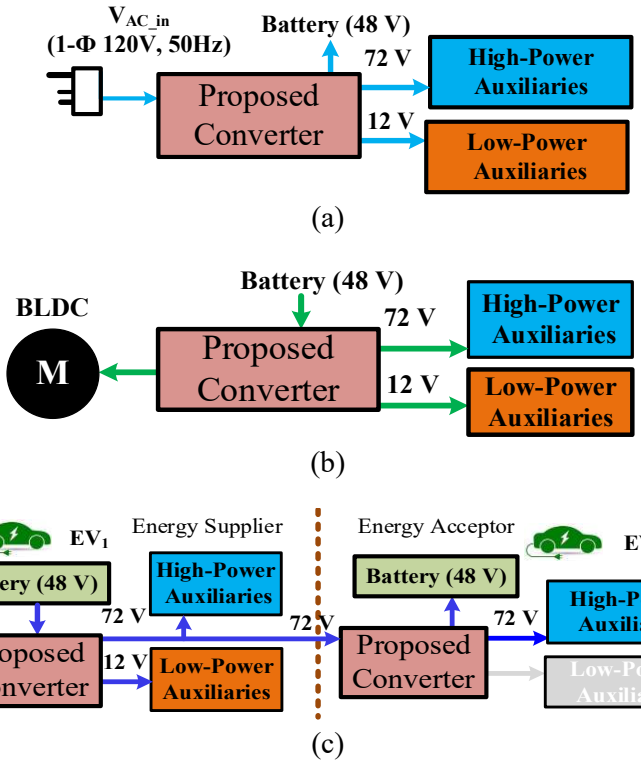

Fig.4. 3 Multioperation of the proposed converter, (a)1-Φ charging, (b) motoring, and (c) V2V charging.

The proposed power converter provides all four functionalities: single-phase charging, motoring mode, vehicle-to-vehicle (V2V) charging, and auxiliary power supply through a single converter.

The block diagram of the proposed idea is shown in Fig.4. 2. Further, the different functionalities achieved by the proposed power converter are shown in Fig.4. 3. The proposed converter is integrated with an on-board charger, multioutput for the auxiliary supply, motoring operation, and vehicle-to-vehicle charging operation, as shown in Fig.4. 3 (a), (b) and (c), respectively. The multioutput features of the proposed converter are utilized for functionalities of V2V charging and auxiliary supplies, along with motoring and single-phase charging.

4.2 Operation proposed on-board power processor

The integrated on-board power processor of multifunctionality for low-power EVs is shown in Fig.4. 4. Along with the single-phase charging, the multioutputs are available in motoring as well as in V2V charging operation.

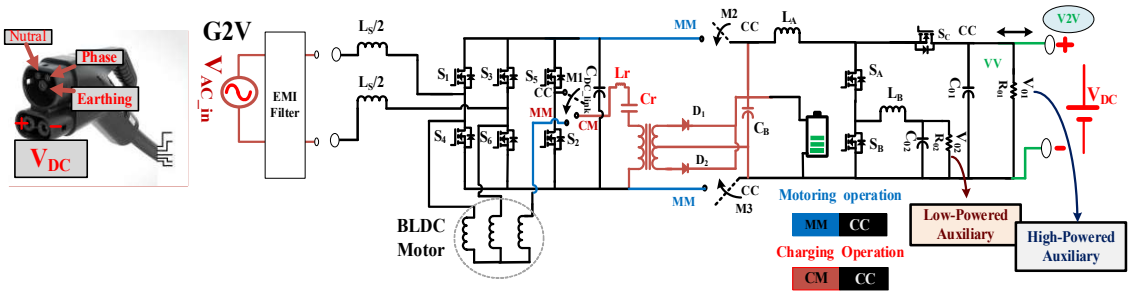

Fig.4. 4 Circuit diagram of the proposed power converter.

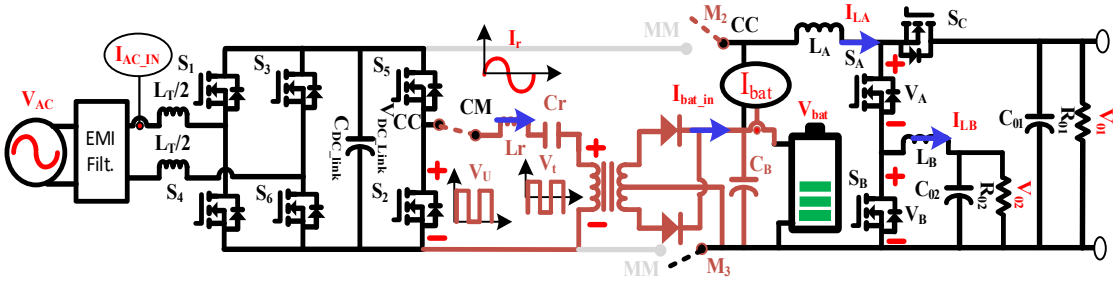

Fig.4. 5 proposed converter during single-phase charging.

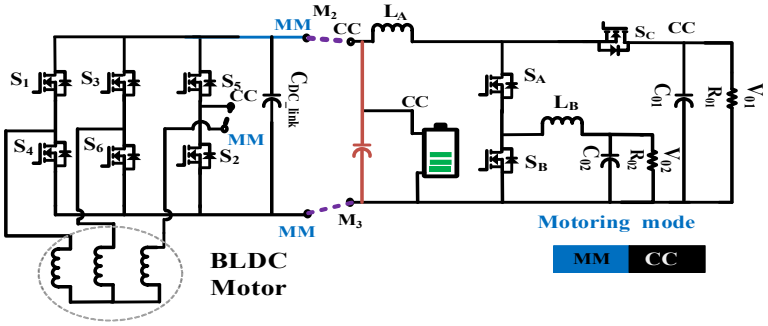

Fig.4. 6 Proposed converter during motoring operation.

One function is transformed into another with the help of only three switches: M_1, M_2, and M_3. Switch M_1 is a single-pole double-throw (SPDT) switch, and M_2 and M_3 are single-pole single-throw (SPST) switches. Their single pole terminal is represented by a common mode connection (CC), and the double-through terminals are represented by a charging mode connection (CM) and motoring mode connection (MM). The switch M1's CC-CM is connected for single-phase charging, and M_2 and M_3 remain open. Further, the power plug is connected

at the front end of the proposed power processor, as shown in Fig.4. 5. In motoring mode operation, switch M_1's CC is connected to MM and the M_2 and M_3 switches CC is connected to the MM connection, as shown in Fig.4. 5. In V2V operation, all the switches are remains open, as shown in Fig.4. 7. The transition between these modes is conducted at a standstill.

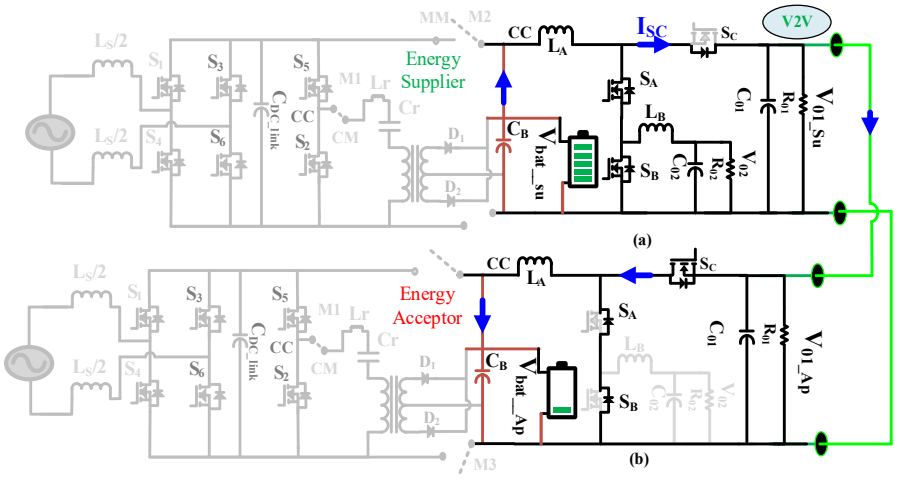

Fig.4. 7 Connection of the proposed converters for V2V charge transfer.

The operation of the proposed converter in different operating modes:

4.2.1 Single-phase charging (M_1 CC-CM)

The proposed converter maintains the unity power factor at the source terminal and charges the battery using a constant-current constant-voltage (CC-CV) charging technique. During the charging, it generates three outputs from the single-phase 120V, 50 Hz power supply. The first DC output of 48 V charges the battery using the CC-CV technique, and the second and third DC outputs of 72 V and 12 V meet the power demand of the EV cabin. The steady-state equation of the charging mode is given in (4.1), (4.2), and (4.3).

The relation between these voltages is stabilized as follows.

$$V_{bat} = \frac{\sqrt{2} * V_{AC\_in} |\sin wt| * g_{DC\_n}}{(1-D) * 2 * n} \tag{4.1}$$

$$V_{01} = \frac{\sqrt{2} * V_{AC\_in} |\sin wt| * g_{DC\_n}}{(1-D) * (1-D_1) * 2 * n} \tag{4.2}$$

$$V_{02} = V_{01} * D_2 \tag{4.3}$$

$$g_{DC\_n} = \left| \frac{L_n * {f_n}^2}{\left[(L_n + 1) * {f_n}^2 - 1\right] + j\left[({f_n}^2 - 1) * f_n * Q_L * L_n\right]} \right|$$

Where: V_{AC_in} (rms) is the source voltage, w is the power line angular frequency, and D is the duty ratio for the switches S_4 and S_6, g_{DC_n} intermediate resonant converter gain, normalized inductance (L_n) is the ratio of magnetizing inductance (L_m) to the leakage inductance (L_r), normalized frequency (f_n) is the ratio of the switching frequency (f_{sw}) of the intermediate switches S_5 and S_2 to the series resonance frequency (f_r) by L_r and C_r, Q_L is the quality factor, and n is the transformer turn ratio. D_1 is the duty ratio of the complete shoot-through (S_A and S_B ON), D_2 is the duty ratio of the power state (S_A ON and S_B OFF), and the remaining time interval represents the zero state of the converter (S_A and S_B OFF).

From the steady state Eq. 1, the battery voltage is independent of the multioutput variables. It depends on the gain of the AC supply voltage and duty ratio D of switches S_4 and S_6, and the intermediate converter gain (g_{DC_n}). The home outlet's AC supply voltage is fixed, and the duty ratio adjusts the DC-link voltage according to the current or voltage at the battery terminal. Further, the value of the intermediate resonant converter gain (g_{DC_n}) is one for the switching frequency (f_{sw}) equal to the resonance frequency (f_r). It eliminates the additional sensor from the DC/DC conversion in the conventional charging controller. It works on series resonance and provides zero-voltage switching (ZVS) in S_5 and S_2 during turn-on time.

The auxiliary power supply is integrated with the charging operation, and it has two control variables, D_1 and D_2, which are defined in equations (4.2) and (4.3) to regulate the boost and buck auxiliary output voltages. The high-power auxiliary output V_{01} is related to V_{bat} and the D_1 duty ratio of the complete shoot-through. The battery voltage remains constant during charging and discharging operations, and the complete-shoot-through duty ratio (D_1) is adjusted according to load variation.

The low-power auxiliary voltage is related to V_{bat}, D_1, and D_2. For a fixed voltage of V_{01}, the effect of D_1 on V_{02} is overcome. The D_2 controls the V_{02} in any variation in the load.

4.2.2 Motoring mode (M_1, M_2, M_3 CC-MM):

Switch off the single-phase power supply and plug out the single-phase connector. After that, switch M1's CC is connected to MM, and the M_2 and M_3 switches CC is connected to the MM connection to form motoring mode, as shown in Fig.4. 6. During the motoring operation, it generates three outputs from the battery. The first output drives the BLDC motor using a High-PWM Low-ON (HPLN) switching technique, where the PWM width controls its speed, while the second (V_{02}) and third (V_{01}) DC outputs power the low and high-power auxiliaries of the EV cabin. The HPLN switching also helps in reducing the commutation torque ripple.

The multioutput of the proposed converter remains the same during the motoring mode operation. Only the energy source has been shifted from the single-phase AC supply to the battery.

4.2.3 Vehicle-to-Vehicle (V2V) charging mode:

During V2V charging, all the additional switches, M_1, M_2, and M_3, are turned off, and the proposed power converter from both of the vehicles is connected for the energy exchange, as shown in Fig.4. 7. The steady-state relation between the connected vehicle voltages is given in (4), (5), and (6).

$$V_{01\_Su} = \frac{V_{bat\_Su}}{(1-D_{1\_Su})} \tag{4.4}$$

$$V_{01\_Ap} = V_{01\_Su} \tag{4.5}$$

$$V_{bat\_Ap} = V_{01\_Ap} * D_C \tag{4.6}$$

Where: V_{01_Su} is a supplier of boost voltage, V_{bat_Su} is the supplier battery voltage, D_{1_Su} is the supplier complete shoot-through interval V_{01_Ap} is the acceptor's terminal voltage, V_{bat_Ap} is the acceptor battery voltage, D_C is the acceptor duty ratio.

The multioutput features of the proposed converter are utilized for functionalities of V2V charging and auxiliary supplies, along with motoring and single-phase charging. Further, the boosted output from the auxiliary power supply is also used for the energy transfer and is expressed by (4). The power converter of the energy acceptor extracts the energy from the boost output of the energy supplier terminal, and its voltage expression is given in (5). Further, this voltage is adjusted by the switch Sc's duty ratio according to the acceptor battery current or voltage requirements, and it is expressed in (6).

4.3 Selection of the circuit parameter for multimode operation

The selection of components for the multifunction integrated on-board power converter is very important. In the selection process of the element, its value is determined in the individual mode of operation. The elements are selected based on their maximum tolerance values to

ensure proper circuit operation. The selection of elements is represented in the sequence of magnetizing inductance, capacitance, resonant tank, and the selection of all the switches.

Table 4. 1 Rating of the selected elements

S.N	Eq.	Charging operation	Motoring operation	Selected Components
(i)	(7)	$L_{Source} = \frac{{V_{AC}}^2}{\%I_{ripple} * P_o * f_{sw}} \left(1 - \frac{\sqrt{2} * V_{AC}}{V_{DC}}\right)$	Not required	2mH (DCR=0.74Ω)
(ii)	(8)	$L_A = \frac{V_{bat} * D1}{f_s * \Delta I_A}$	$L_A = \frac{V_{bat} * D1}{f_s * \Delta I_A}$	1mH (DCR=0.37Ω)
(iii)	(9)	$L_B = \frac{(V_{bat} - V_{02}) * D_2}{f_s * \Delta I_B}$	$L_B = \frac{(V_{bat} - V_{02}) * D_2}{f_s * \Delta I_B}$	0.8mH (DCR=0.7Ω)
(iv)	(10)	$C_{dc_{link}} \geq \frac{2 * P_o * t_{hold}}{{V_o}^2 - {V_{min}}^2}$, $C_{dc\_link} \geq \frac{P_o}{2 * \pi * f_{line} * \Delta V_o * V_o}$	Used as a filter	3mF(ESR=1.05Ω)
(v)	(11)	$C_{01} = \frac{V_{bat} * D1}{f_s * R_{01} * \Delta V_{01}}$	$C_{01} = \frac{V_{bat} * D1}{f_s * R_{01} * \Delta V_{01}}$	470μF(ESR=0.15Ω)
(vi)	(12)	$C_{02} = \frac{V_{bat} * (1 - D1 - D_2) * D_2}{8 * {f_s}^2 * (1 - D_1) * \Delta V_{02} * L_B}$	$C_{02} = \frac{V_{bat} * (1 - D1 - D_2) * D_2}{8 * {f_s}^2 * (1 - D_1) * \Delta V_{02} * L_B}$	100μF(ESR=0.1Ω)
(vii)	(13)	$f_r = 1 \Big/ 2 * \pi \sqrt{(L_r * C_r)}$	Not required	32μH, 2 μF
(viii)	(14)	All switches and three additional switches (M_1, M_2 and M_3)		650 V, 32 A 450 V, 30 A

V_{ac} is RMS input voltage; $\%R_{ripple}$ is the percentage of inductor ripple current regulation; P_o is maximum steady state power; f_{sw} is switching frequency, V_{bat} *is* the battery voltage, D_1 and D_2 are the duty ratio of the complete shoot-through and power state, f_s is the switching frequency of the S_A and S_B, and ΔI_A, ΔI_B are the leakage current ripple in inductor L_A and L_B, respectively, V_{DC_link} is DC-link voltage. t_{hold} is hold-up time, V_{min} is the minimum voltage to which the output voltage is allowed to drop, f_{line} is the input line frequency, and ΔV_o is the specified voltage ripple. V_{01} is the boost output, and V_{02} is buck output of the multioutput. Where: ΔV_{01}, ΔV_{02} are the voltage ripple in the capacitor C_{01} and C_{02}, respectively.

4.3.1 Selection of the magnetizing inductance

The magnetizing inductances are selected to minimize the current ripple during their respective operating modes. The source inductance minimizes the ripple current during charging mode, which helps with power factor correction. The maximum inductor current ripple determines the rating of the source inductor to ensure that the converter operates in continuous conduction mode. The value of the inductor is calculated from the (7) as shown in L_A and L_B inductances are determined by the maximum current ripple limit during complete shoot-through and power state for the multioutput operation. They are expressed in Table 4.1 by (8) and (9), respectively.

4.3.2 Selection of the capacitance:

Capacitors are selected to minimize the voltage ripple in their respective mode of operation. The DC-link capacitor filters out the voltage ripple during charging mode and reutilizes it to filter out the switching ripple during motoring mode operation. The rating of the DC-link capacitor is determined by hold-up time and voltage ripple limitation. The hold-up time is typically taken as one and a half cycles of the power frequency. The greater value of the capacitor should be considered from (10), as shown in . To optimize its size, field windings of the BLDC motor have been added C_{01} and C_{02} capacitances of the proposed converter are

determined by the maximum voltage ripple limiting during complete shoot-through and the zero state for multioutput operation. They are expressed by (11) and (12) in Table 4.1, respectively.

4.3.3 Selection of the component in the intermediate resonant converter:

In the intermediate section, switches S_5 and S_2 operate at series resonance and reduce the control complexity for the battery charging. Further, in motoring operation, attached to the front-end switches S_1, S_4, S_3, and S_6 drive the BLDC motor. For the component selection, first, select the resonant frequency and design a transformer with leakage inductance (Lr) that is capable of operating at the rated current, and then the resonant capacitor (C_r) is chosen according to the voltage. The operating resonant frequency of the converter is 20 kHz, and according to that, the values of Lr and Cr are shown in (13) of Table 4.1.

4.3.4 Selection of all the switches:

The switches S_1, S_3, S_5, S_4, S_6, and S_2 should operate at high voltage and current. The selected switch is IPW60R040CFD7, which can operate at 650 V and 32 A. The selected diode is RURG8060, which can operate at 80 A, 600V, and the switches S_A, S_B, and S_C are IPW60R040CFD7, selected according to the future scope for the higher power EVs. M_1, M_2, and M_3 are selected for the effective operation during the voltage and current stress in their respective modes. During charging mode operation, the DC-link voltage (470 $V_{DC\text{-}MAX}$) appears on all these switches. During the motoring mode operation, 30 A (max) is drawn from the battery for driving the BLDC, which goes through these switches. The rating of these selected switches is shown in (14) of Table 4.1.

4.4 Control algorithm of the proposed converter:

The proposed converter is designed based on the rated power, within which the voltage regulation is unaffected, irrespective of the load variation. All the available voltages have a suitable control system to coordinate the power flow between the different loads. The rated power and the voltage level in their individual mode of operation are represented in Table 4. 2 Further, the multimode control algorithm is explained along with multioutput operation. The control logic for all these operations is shown in Fig.4. 8. Nine sensing parameters have been used for all these operating modes, which are appropriately tuned to prevent unintended control loop behaviour. Six sensing perimeters, V_{bat}, I_{bat}, V_{in}, I_{in}, V_{01}, and V_{02}, have been used for charging and the auxiliary power supply, and three sensing parameters of the hall effect sensors H_1, H_2, and H_3 have been used for the motor drive. The modes are selected by the three

additional switches, M_1, M_2, and M_3, and the controller operates according to the selected mode.

4.4.1 Control logic for single-phase charging:

Table 4. 2 Specification of the power level in their respective modes of operation

Mode of operation	Power IN	Voltage and Current rating at the load			Output Power (Watt)
Charging	V_{in}= 120 V, I_{in} = 6.5 A (1-Φ AC source)	V_{bat}= 48V, I_{bat} = 5.5 A (Battery as a load)	V_{01}=72 V, I_{01} =5.5 A (High-power auxiliary load)	V_{02}=12 V, I_{02} = 5A (Low-power auxiliary load)	264+396+60 = 720
Motoring	V_{bat} = 48 V I_{bat} = 21 A (Battery as a source)	V_{BLDC}=48 V, I_{BLDC} =10 A (BLDC motor as a load)	V_{01}=72 V, I_{01} =5.5 A (High-power auxiliary load)	V_{02}=12 V, I_{02} =5 A (Low-power auxiliary load)	480+396+60 =936
V2V	V_{bat} = 48 V I_{bat} = 10 A (Battery as a source)	---	V_{01}=72 V, I_{01} =5.5 A (High-power auxiliary load)	V_{02}=12 V, I_{02} =5 A (Low-power auxiliary load)	396+60= 456
V_{bat} and I_{bat} (battery voltage and current), V_{01} and I_{01} (High-power auxiliaries' voltage and current), V_{02} and I_{02} (Low-Power auxiliaries' voltage and current), V_{BLDC} and I_{BLDC} (motor voltage and current rating),					

Two independent loops have been used in single-phase charging to avoid the coupling effect. The first controller maintains the unity power factor at the source terminal and charges the battery with a constant-current constant-voltage technique, as shown in Fig.4. 8(a). Further, the second controller maintains the regulated auxiliary power supplies to the EV cabin, as shown in Fig.4. 8(b).

4.4.1.1 Controller I:

In the first controller, the outer voltage control (PI_1) and the inner current control (PI_2) work in a cascade, in which one controller acts as the set point for another controller to maintain coordination.

a) Voltage control loop (PI_1):

Four sensing parameters, V_{bat}, I_{bat}, V_{in}, and I_{in}, are used for CC-CV charging with a unity power factor at the source terminal. The CC-CV charging technique is used for the battery's long life. In this charging technique, the battery's 80 to 90 percent State of Charge (SOC) is charged through the CC method, and the remaining SOC of the battery is charged

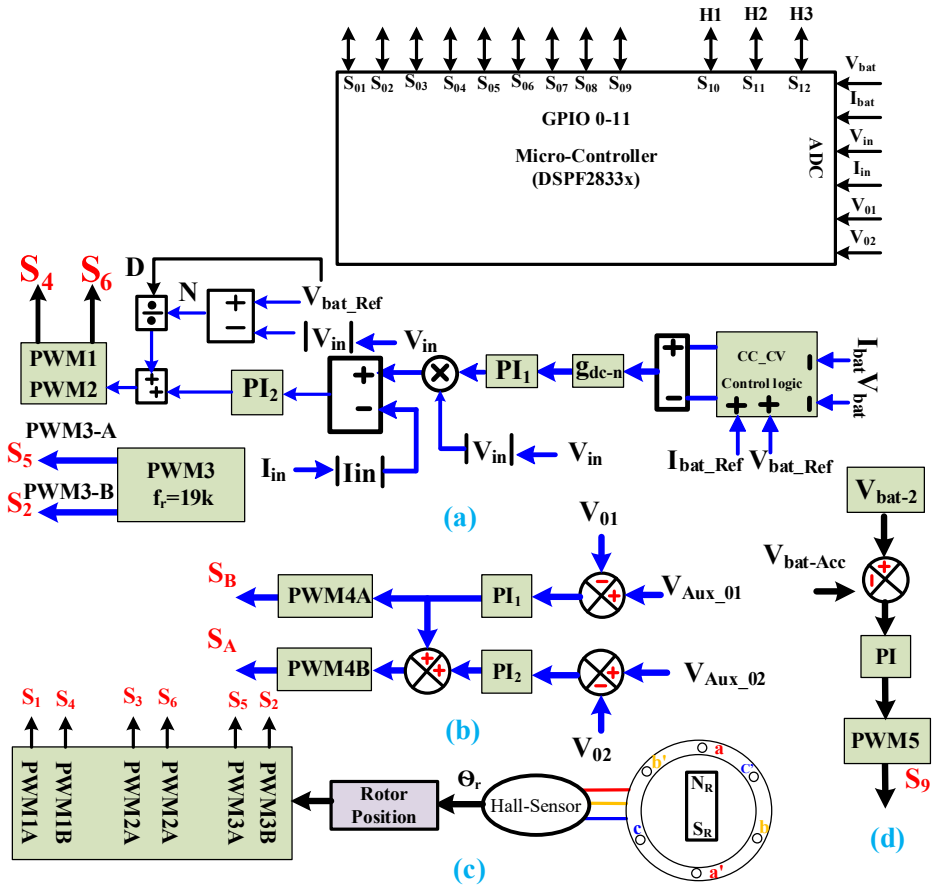

Fig.4. 8 control logic of the proposed system, (a) for the power factor correction, (b) for the regulated auxiliary power supply voltage, (c) BLDC motor drive operation, and (d) acceptor vehicle control logic.

through the CV method. The output of the CC-CV logic is to be an input to the resonant converter. The gain of the resonant converter is one for switching the S_5 and S_2 at the nominalized frequency ($f_n = \frac{f_{switching}}{f_{resonance}}$). It also provides zero-voltage switching during the ON time. Further, the value of the PI_1 controller is determined by the $\frac{\hat{V}_{bat}}{\hat{I}_{in}}$ voltage control transfer function. The bandwidth of this transfer function is 5 Hz, at a phase margin of 60^0, which can easily filter out the double-line power frequency but affects the dynamic operation. The digital controller improves the dynamic compensation during load jumps for better output regulation.

b) Current control loop (IP_2)

The controlling parameters of the PI_2 controller are obtained by the $\frac{\hat{\imath}_{in}}{\hat{D}}$ transfer using small signal analysis for power factor correction. The bandwidth of the transfer function is kept below or equal to 10 % of the switching frequency, and here, it is 2 kHz at a phase margin of 60^0, and

GM of infinity. The output of the current controller loop's closed-loop duty ratio is added to the feedforward open-loop duty ratio. The generated pulse for the switches S_4 and S_6 by summation of the closed-loop duty and the feedforward open-loop duty charges the DC-link capacitor according to the load at the battery terminal. If the load increases, then the duty ratio increases to increase the charge on it, and decreases with a decrease in the load. This duty ratio generates the pulse for switches S_4 and S_6 to perform PFC and CC-CV charging.

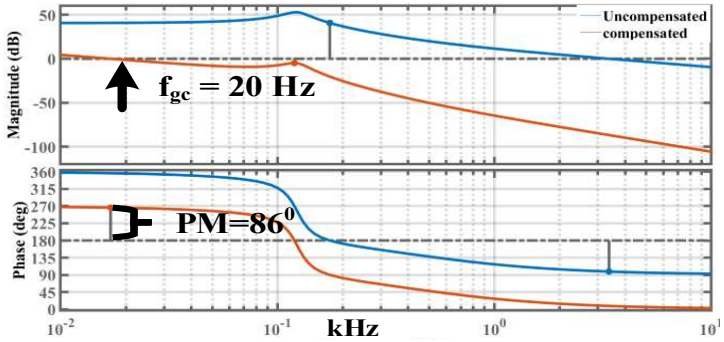

Fig.4. 9 Bode plot of the uncompensated and compensated high-power auxiliary voltage.

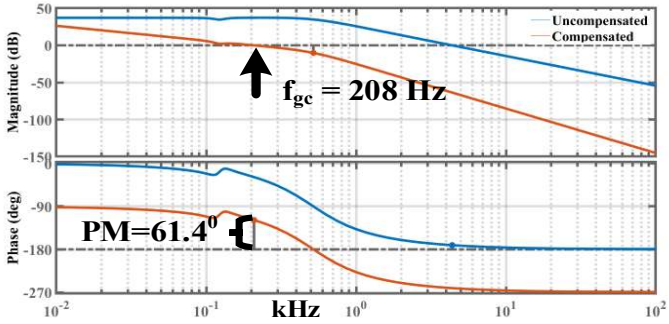

Fig.4. 10 Bode plot of the uncompensated and compensated of low-power auxiliary voltage.

4.4.1.2 Controller II

Controller II is mutually exclusive from Controller I, as shown in Fig.4. 8(b). The Controller II maintains regulated voltages for the high-power and low-power auxiliaries. The small signal analysis of the auxiliary power supply is given in Eq.4.7. The error of the high-power auxiliary terminal is corrected by the PI_1 controller, which is tuned by the $\frac{\hat{V}_{01}}{\hat{D}_1}$ transfer function, and the bandwidth is 20 Hz at a phase merging of 86^0 at the GM of 4.87 dB, as shown in Fig.4. 9. The PI_1 controller output is added to the PI_2 controller output, which is tuned by the $\frac{\hat{V}_{02}}{\hat{D}_2}$ transfer function, with a bandwidth of 208 Hz, at a phase margin of 61.4^0 and a GM of 10.2 dB, as shown in Fig.4. 10. The $\frac{\hat{V}_{01}}{\hat{D}_1}$ and $\frac{\hat{V}_{02}}{\hat{D}_2}$ transfer functions are given in Eqs. 4.8 and 4.9.

$$\begin{bmatrix} \dot{\hat{i}}_{LA} \\ \dot{\hat{i}}_{LB} \\ \dot{V}_{C01} \\ \dot{V}_{C02} \end{bmatrix} = \begin{bmatrix} 0 & 0 & \frac{-(1-D_1)}{L_A} & 0 \\ 0 & 0 & \frac{D_2}{L_B} & \frac{-1}{L_B} \\ \frac{(1-D_1)}{C_{01}} & \frac{-D_2}{C_{01}} & \frac{-1}{R_{01}C_{01}} & 0 \\ 0 & \frac{1}{C_{02}} & 0 & \frac{-1}{R_{02}C_{02}} \end{bmatrix} \begin{bmatrix} \hat{i}_{LA} \\ \hat{i}_{LB} \\ V_{01} \\ V_{02} \end{bmatrix} + \begin{bmatrix} \frac{V_{01}}{I_{A}} \\ 0 \\ \frac{-i_{LA}}{C_{01}} \\ 0 \end{bmatrix} D_1 + \begin{bmatrix} 0 \\ \frac{V_{01}}{L_B} \\ \frac{-i_{LB}}{C_{01}} \\ 0 \end{bmatrix} \widehat{D_2} + \begin{bmatrix} \frac{1}{L_A} \\ 0 \\ 0 \\ 0 \end{bmatrix} \widehat{V_{in}}$$

(4.7)

$$\left[\frac{\hat{V}_{01}}{\hat{D}_1}\right]_{\hat{D}_2=0} = \frac{n_3 S^3 + n_2 S^2 + n_1 S^1 + n_o}{S^4 + d_3 S^3 + d_2 S^2 + d_1 S^1 + d_o} \quad (4.8)$$

$$\left[\frac{\hat{V}_{02}}{\hat{D}_2}\right]_{\hat{D}_1=0} = \frac{a_2 S^2 + a_1 S^1 + a_o}{S^4 + d_3 S^3 + d_2 S^2 + d_1 S^1 + d_o} \quad (4.9)$$

where: $n_3 = -\frac{i_{LA}}{C_{01}}, n_2 = \frac{V_{01}(1-D_1)}{L_A C_{01}} - \frac{i_{LA}}{C_{01}C_{02}R_{02}}, n_1 = \frac{V_{01}(1-D_1)}{L_A C_{01}C_{02}R_{02}} - \frac{i_{LA}}{C_{01}C_{02}L_B}, n_o = \frac{V_{01}(1-D_1)}{L_A L_B C_{01}C_{02}}$,

$a_2 = \frac{V_{01}}{L_B C_{02}}, a_1 = \frac{V_{01}}{L_B C_{02}C_{01}R_{01}} - \frac{i_{LA}D_2}{L_B C_{01}C_{02}}, a_0 = \frac{(1-D_1)^2 V_{01}}{L_A L_B C_{01}C_{02}}, d_3 = \frac{1}{R_{01}C_{01}} + \frac{1}{R_{02}C_{02}}$,

$d_2 = \frac{1}{R_{01}C_{01}R_{02}C_{02}} + \frac{{D^2}_2}{L_B C_{01}} + \frac{1}{L_B C_{02}} + \frac{(1-D_1)^2}{L_A C_{01}}, d_1 = \frac{{D_2}^2}{L_B C_{01}C_{02}R_{02}} + \frac{1}{L_B C_{02}C_{01}R_{01}} + \frac{(1-D_1)^2}{L_A C_{01}C_{02}R_{02}}, d_0 = \frac{(1-D_1)^2}{L_B L_A C_{01}C_{02}}$

$$\left[\frac{\hat{V}_{bat-acc}}{\hat{D}_C}\right] = \frac{S^1}{S^2 + \frac{S^1}{R_{01}C_{01}} + \frac{1}{L_A C_{01}}} \quad (4.10)$$

The output of the PI_1 controller generated a pulse for the switch S_B, and the summation of PI_1 and PI_2 controller outputs generated the pulse for switch S_A.

4.4.2 Control logic for the motoring mode operation

The speed of the BLDC motor is controlled by two main methods: 1) Voltage control and 2) PWM control. In voltage control, the speed of the BLDC is directly proportional to the applied voltage[112]. While in the PWM control scheme, the speed of the motor is controlled by the duty cycle of the applied PWM. An increase in turn-on time raises the average voltage, thereby increasing the motor's speed. Conversely, reducing the turn-on time of the PWM decreases the motor's speed.

The controller in Fig.4. 8(c) performs the motoring mode operation, and controller II for the cabin power supply remains active as same as in single-phase charging mode. The speed

controller determines the rotor's exact position by the three hall effect sensors: H_1, H_2, and H_3, and the inverter is excited according to that position to create a revolving field by High-PWM Low-ON switching. The high PWM switching in S_1, S_3, and S_5 of the upper leg of the inverter changes the average voltage applied to the motor. The lower switches S_4, S_6, and S_2 are turned on in their respective time intervals.

4.4.3 Control logic for the V2V charging:

For V2V charging, the proposed power converter from both vehicles is connected. The controller for the energy supplier vehicle remains the same as the auxiliary power supply, as explained in the single-phase charging of Fig.4. 8(b), and the energy acceptor vehicle controller is given in Fig.4. 8(d). The auxiliary power of the energy supply vehicle is active during energy exchange time. The energy acceptor vehicle controller is designed by the $\frac{\hat{V}_{bat-A}}{\hat{D}_c}$ transfer function is given in Eq. 4.10. The high-power auxiliary voltage of 72 V is bucked according to the acceptor vehicle's required battery voltage and charged with the desired current rate.

Table 4. 3 Comparative analysis with similar prior work

L.No.	Multifunction (Efficiency)		M-Out	V2V (480 W)	Requirement of Auxiliary Battery & its charger		Function	Galvanic isolation	Switches		Additional Switch for Mode Transfer	Total Switches
	OBC (780 W)	MM (1 kW)			12 V	Charger			MOSFET	Diode		OBC
[87]	✓(91)	×	×	×	✓	✓	**1**	✓	8	12	3	**23**
[113]	✓*	×	✓	×	✓	×	**2**	×	14	4	0	**18**
[114]	✓(89.9)	✓	×	×	✓	✓	**2**	×	6	4	4	**14**
[49]	✓(90)	✓(94)	×	×	✓	✓	**2**	✓	20	0	4	**24**
[64]	✓**	×	×	✓(91.5)	✓	✓	**2**	×	8	0	0	**8**
P.C	✓(91.9)	✓(92.3)	✓	✓(93.2)	×	×	**4**	✓	9	2	3	**14**

L.No.= Literature number, OBC=on-board charger, MM=motoring operation, M-out=multioutput, "✓*" completer on-board charging efficiency not given, "✓**" efficiency is not given,

4.5 Comparative analysis of the proposed converter

Comparative analysis of the proposed converter is described in two methods: 1) differences in their functioning and specifications with similar prior work, and 2) cost comparison with them. Comparative analysis with the existing converters is given in Table 4. 3.

Comparative analysis with the existing converter is expressed with multifunction, multimode, and multioutput functions. In [87], the integrated converter provides a wide range of output for battery charging with three additional switches, with an efficiency of 91%. However, this system requires two additional converters for the basic operation of the EV: one

for charging the low-power auxiliary battery and another for driving the motor. In [113], the auxiliary power module (APM) is integrated with the on-board charger and charges the main battery and the LV battery simultaneously. However, 18 switches are used for this operation. Nevertheless, a separate converter is still needed for motoring operations. In [114], the integrated converter performs multifunction operations, enabling the on-board charger to charge the main battery with an efficiency of 89.9% and also drives the motor. These functionalities are achieved using 10 switches and four additional switches, but the on-board charger lacks galvanic isolation. In [49], the integrated isolated on-board charger supports both charging and motoring operations with efficiency of 90% and 94%. However, in both [114] and [49], a separate converter is required for low-power auxiliary battery charging. The above-mentioned converter either performs the multifunction operation or provides the multioutput for charging the additional low-power auxiliary battery.

An additional bi-directional converter is required for vehicle-to-vehicle charging operation in the above-mentioned converter. In [64], for the multimode operation, the neutral point of the motor winding and the negative rail of the two on-board chargers are connected for V2V charging. It performs V2V charging with an efficiency of 91.5%. However, access to the motor winding's neutral point is essential for multimode operation, which can increase the machine design complexity. However, a higher switch count can increase the switching loss. In the proposed system, only six switches are active while V2V charging.

Table 4. 4 Cost comparative analysis

S. N	Component	Conventional System				Proposed System	
		MM [114]	**CM**[114]	**V2V** [64]	**Total (USD)**	**Com.**	**Total (USD)**
1.	Switch, Diode	6,4		4	10×11+4×4	9,2	9×11+2×4
3.	Gate-driver Accessories	6		4	10×3+10	9,2	9×3+10
2.	Heat-Sink	1		1	2×20	1	1×20
4.	12V Battery	1			32	0	0
5.	12 V Charger	1			10	0	0
6.	PCB	1		1	2×62	1	62
7.	Additional switch	4		0	4×7	3	3×7
Total Cost (in $)					400		247

The cost comparative analysis of the proposed converter is given in Table V. For motoring mode (MM) and charging mode (CM) operation,[114] has been chosen for comparison because it has a minimum number of switches, i.e. 14, amongst prior works for MM and CM mode. Similarly, for comparison in V2V mode, [64] has been chosen because it has a minimum number of switches, i.e., 4 for V2V mode.

Table 4. 4 presents a cost comparison between the proposed converter with the existing converter. The switches (IPW60R040CFD7), diode (RURG8060), gate driver (FOD3184), heat sink (1960012091T00S), PCB (FR4 epoxy glass), absorbent glass mat battery of 12 V (Mahindra & Mahindra), and relay (V23076-A3001-C132) are the names of the components utilized for this analysis. The suggested solution would set you back 261 USD, whereas the standard converter will set you back 400 USD altogether. The suggested technique saves about USD 159 in costs.

4.6 Efficiency analysis of the proposed converter

In power electronics converters, the main losses are switch losses, inductor loss, diode loss, transformer loss, capacitor series resistance loss, inductor direct current loss, and other losses. These losses are represented in Table 4. 5.

Table 4. 5 Formulation of the basic power electronics converter losses

Elements	Losses
Switch loss	$P_{sw} = \frac{V_{in}I_{in}(t_r+t_f)f_{sw}}{2}$,$P_c = R_{DS(ON)} * {I_{in}}^2$(rms)
Inductor loss	$P_{ind} = DCR * {I_{in}}^2$(rms)
Diode loss	$P_{D(cond)} = V_f * I_f$, $P_{D(rev.lek)} = V_r * I_r$, $P_{D-sw} = \frac{V_f I_f (t_r) f_{sw}}{2}$
Transformer loss	$P_{T(cond)} = {I_{in}}^2$(rms)* R_{Turn}, $P_h = \eta * {B_{max}}^n f * V$,$P_{eddy} = K_e * {B_{max}}^2 * f^2 * t^2 * V$
Capacitor loss	$P_{C-L} = ESR * {I_{in}}^2$(rms)
Gate driver loss	$P_{gate}=Q_g*V_{gate}*f_{sw}$, $P_{static}=V_{DC}*I_q$
Where: Psw (switching losses), Vin (Input voltage), Iin (input current), tr (rise time), tf (fall time), fsw (switching frequency), Pc (Switch conduction loss), RDS (swich conducting resistance),Pind (inductor loss), DCR (inductor direct current resistance), $P_{D(cond)}$ (Diode forward conduction loss), $P_{D(rev.lek)}$ (Diode reverse conduction loss), P_{D-SW} (Diode switching loss), $P_{T(cond)}$ (Transformer conduction loss), P_h(Transformer hysteresis loss), P_{eddy} (Transformer eddy current loss), ESR (capacitor equivalent series resistance).P_{gate} (gate charge energy consymption), Q_g (gate charge), V_{gate}(driver turn-on votlage), P_{static}(static power consumption in gate driver), V_{DC}(supply voltage of the gate driver), Iq (quiescent current)	

Table 4. 6 Loss during single-phase charging operation

Loss Distribution	Single-phase charging (780 W)
Front-end converter	15.34
Resonant tank	2.13
Transformer	0.832
Multioutput	33.6
Other loss	11.19
Total Loss	63.29
Output Power	716

4.6.1 Loss analysis of charging mode operation:

In charging mode, a total of 12 switches operates in the active state. Among them, eight switches function in hard switching, two diodes experience conduction and switching losses, and two switches operate under zero-voltage switching (ZVS). Other losses are transformer loss, multioutput converter loss, and other losses like EMI and EMC loss. The converter operating power is shown in Table 4. 6. Further, their loss distribution is shown in Fig.4. 11.

Efficiency of the proposed converter during charging mode is

$$= (780\text{-}63.29)/780=0.9188$$

$$= 91.88\ \%$$

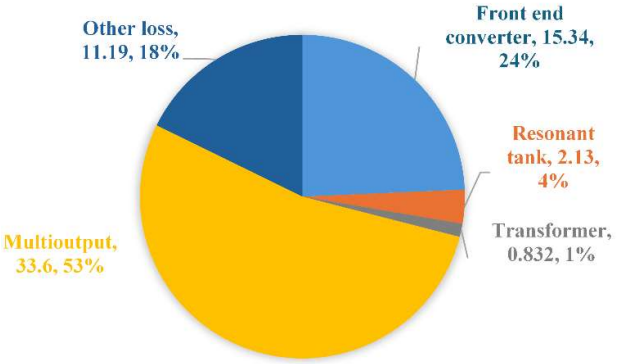

Fig.4. 11 Map of the proposed converter loss distribution during charging mode.

Table 4. 7 Loss during motoring mode (MM) operation

Loss Distribution	MM (1000 W)
Switching	28.24
Filter	3.95
Multioutput	33.6
Other loss	10.65
Total losses	76.44
Power used	923.55

4.6.2 Loss Analysis of Motoring Mode Operation

In motoring mode, a total of 12 switches are operated. The front six switches, S_1, S_2, S_3, S_4, S_5, and S_6, are operated with High-PWM Low-ON switching. The DC link capacitor of the charging mode operates as a filter capacitor in motoring mode, which produces capacitor equivalent series resistance conduction loss, multioutput converter loss, and other losses, such

as EMI and EMC, etc. The operating power and its respective losses are listed in Table 4. 7. Further, their loss distribution is shown in Fig. 13.

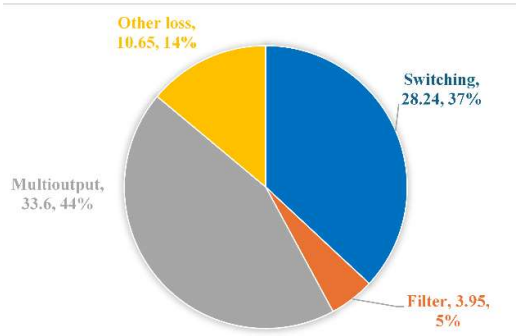

Fig.4. 12 Map of the proposed converter loss distribution in motoring mode.

Efficiency of the proposed converter during motoring mode operation is

= (1000-76.44)/1000=0.923

= 92.3 %

Table 4. 8 Proposed converter loss during V2V charging

Loss Distribution	**V2V (480 W)**
S_A	17.12
S_B	9.28
L_{A+B}	1.18
C_{01+02}	0.52
S_C	4.21
Other Loss	1.28
Total Loss	33.59
Output Power	446.4

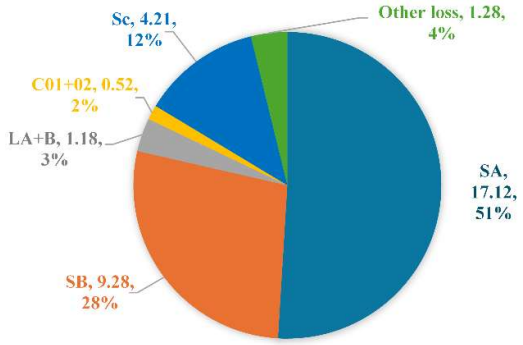

Fig.4. 13 Map of the proposed converter loss distribution during V2V charging.

4.6.3 Loss analysis of V2V charging operation:

For V2V charging, the proposed power converter from both vehicles is directly connected, and only six switches remain in the active state. For the efficiency analysis, only the energy supplier Vehicle is considered. The loss analysis is determined by the switching loss

in S_A and S_B switches with one diode, and the filer capacitor and the inductor loss with the other loss are considered. During V2V operation, the operating power and its operational losses are listed in Table 4. 8. Further, the loss distribution during V2V operation is expressed in Fig.4. 13.

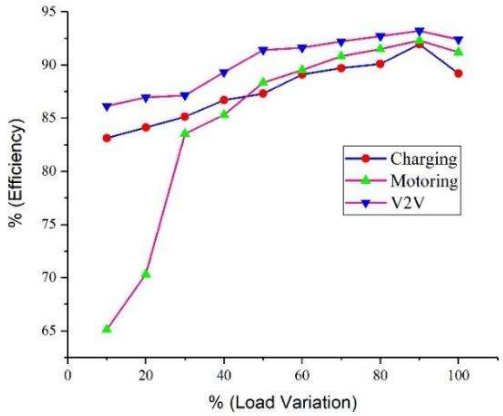

Fig.4. 14 Efficiency curve of all the modes of operations.

The loss analysis of the proposed converter is expressed through the pie chart in their individual mode of operation. In this efficiency analysis, the new analysis is added to the previous because previously, the loss is given at a particular load, but now efficiency is taken by varying the load from 10% to 100%. An efficiency graph of the proposed power converter is given in Fig.4. 14.

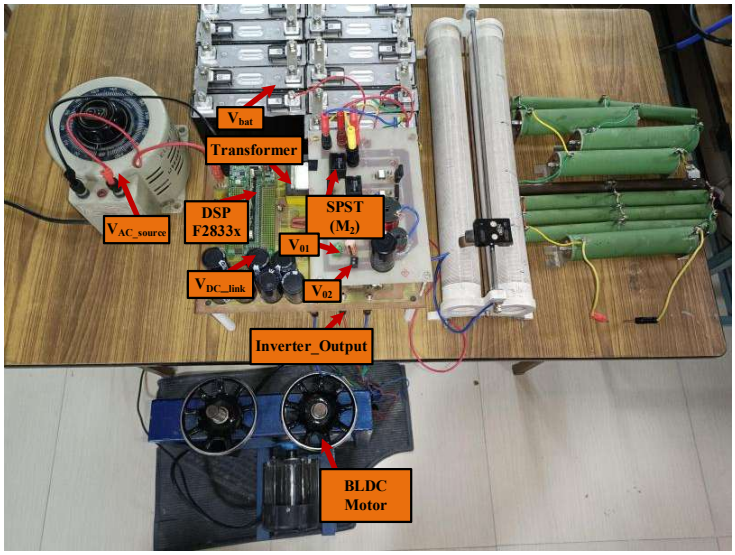

Fig.4. 15 Photograph of an experimental prototype of the proposed converter.

4.7 Experimental validation

The experimental result of the proposed converter is expressed with integrated on-board chargers with their different functionalities. In its multifunction, it performs single-phase

charging, motoring, V2V charging, and multioutput. The multioutput features of the proposed converter are utilized for functionalities of V2V charging and auxiliary supplies, along with motoring and single-phase charging. The pictorial representation of the proposed converter is shown in Fig.4. 15.

4.7.1 Multifunction operation of the proposed converter:

4.7.1.1 Charging operation with auxiliary power supply

In the charging operation, it maintains the unity power factor at the source terminal and charges the battery from the 120 V, 50 Hz single-phase power supply. During the charging, it generates three outputs; the first DC output charges the 48 V battery, and the second and third outputs of 12 V (V_{02}) and 72 V(V_{01}) meet the power demand of the cabin.

a) UPF with multioutput during charging operation:

According to the industry standard IEC61000-3-2, during single-phase charging, the PF should be greater than 0.98. During the single-phase AC charging, source voltage and current are in phase with 0.99 power factor (PF), and the multioutputs are shown in Fig.4. 16.

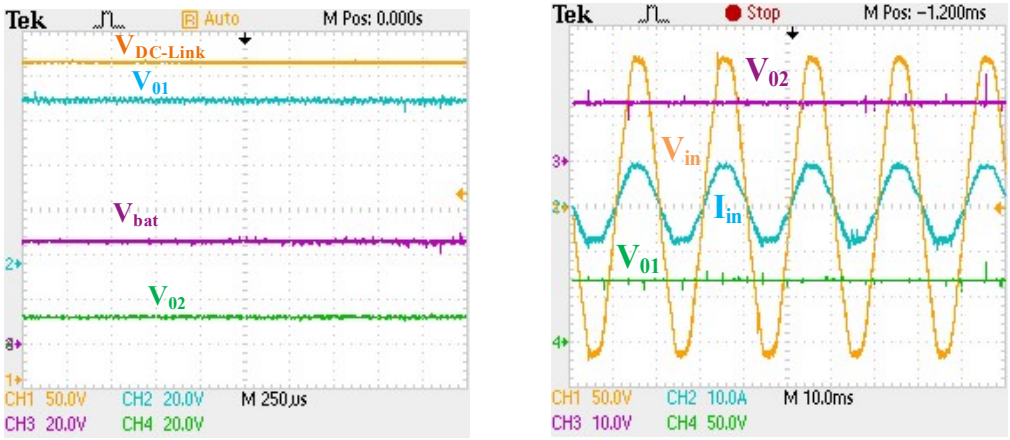

(a) (b)

Fig.4. 16 During AC charging, (a) available output voltages for battery and cabin's power demand and (b) unity power factor with the auxiliaries' voltages.

DC-link voltage ($V_{CD\text{-}Link}$), battery voltage (V_{bat}), and the available auxiliary voltages V_{01} and V_{02} are shown in Fig.4. 16(a). Further, the single-phase AC power supply source voltage (V_{IN}) is in phase with the source current (Iin), and the auxiliary voltages (V_{01} and V_{02}) for the power support of the EV cabin are shown in Fig.4. 16(b).

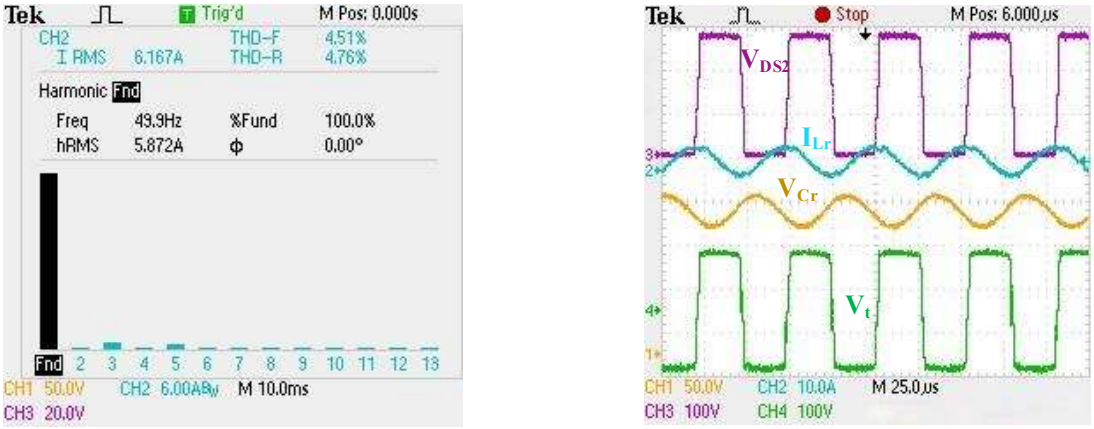

(a) (b)

Fig.4. 17 (a) THD spectrum of the source current and (b) intermediate resonant converter operation during series resonance

b) THD spectrum of the source current and operation of the intermediate resonant converter

The amplitude of the source current, with its respective harmonics, is shown in Fig. 18(a). According to the IEEE 519-2014, the THD value should be less than 5% [115]. The Total Harmonic Distortion (THD) as a percentage of the root mean square value of the source current is 4.76 %, and the percentage of the fundamental RMS value of the source current is 4.51 %. The resonant tank of the proposed converter works at a normalized frequency and provides unity gain with ZVS during turn-on time while single-phase charging. During the resonance, sinusoidal current (I_{Lr}) flows through the circuit, and unipolar (V_U) and bipolar voltage (Vt) appear at the switch S_2 and the transformer terminal, respectively, as shown in Fig. 18(b).

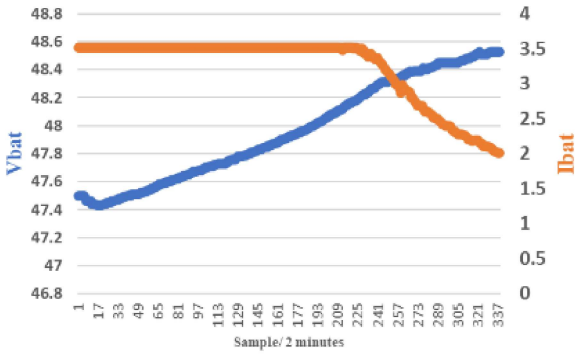

Fig.4. 18 CC-CV charging operation

c) CC-CV charging technique

A graph plotted between battery voltage and current data, which is taken every two minutes, is shown in Fig.4. 18. The constant current 3.5 A charges the 48 V battery until the set point of

the CC to CV transition. After the set point of 48.2 V, the constant voltage is applied for the remaining state of charge (SOC), and the current starts to fall.

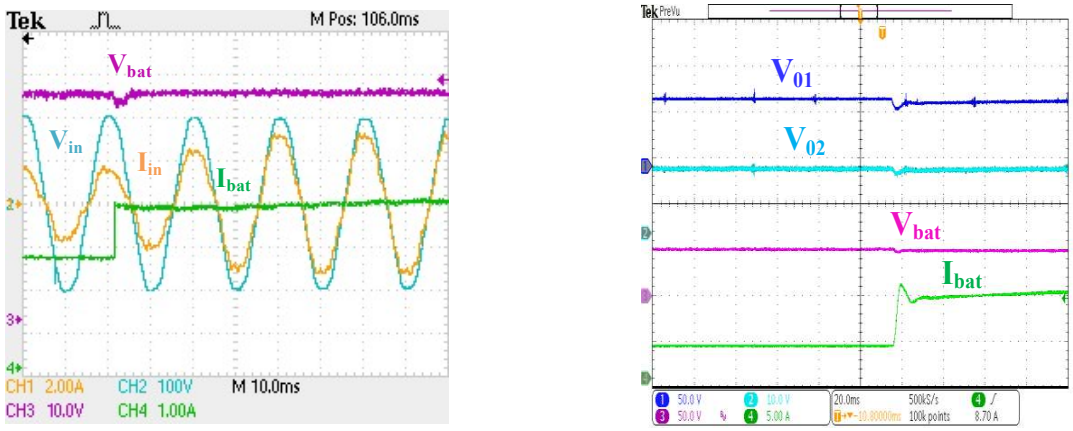

(a) (b)

Fig.4. 19 In single-phase charging, (a) the power factor (PF) at the source terminal is maintained during load dynamics, and (b) the available voltage is sustained after load dynamics are applied at high-power auxiliary.

d) 4.7.1.1.4 Voltage regulation of charging mode during load dynamics

For the dynamic analysis of the proposed converter during charging mode, a load dynamic is applied at the auxiliary terminal voltages, and the converter performance is analyzed, as shown in Fig.4. 19. Fig.4. 19(a) represents that the proposed converter maintains the unity power factor at the source terminal, irrespective of a load variation. V_{in} and I_{in} represent the input current and voltage, and V_{bat} and I_{bat} represent the battery voltage and current during load dynamics in on-board charging. Fig.4. 19(b) shows the voltage regulation of available output voltages of the proposed power converter during on-board charging, irrespective of the variation of the load.

4.7.1.2 Motoring mode operation with the auxiliary power supply

In motoring mode, the proposed converter restructures itself and drives the Brushless DC motor from the 48 V main battery. During this operation, it also generates two more outputs, voltages 12 V (V_{02}) and 72 V (V_{01}), for the power support of the EV cabin.

a) Motor current during the load torque:

The motor is driven with the battery using an existing HPLN switching scheme, where the upper leg is driven with PWM, and the lower leg is driven with 120 degrees ON. Fig. 21(a) represents the motor line current I_a, I_b, and I_c with battery voltage during its loading condition, and Fig. 21(b) represents the input current of the inverter with a drain-to-source switching

voltage of the upper leg of the inverter. These voltages are V_{A_DS}, V_{B_DS}, and V_{C_DS}, which are 120 degrees phase apart from each other.

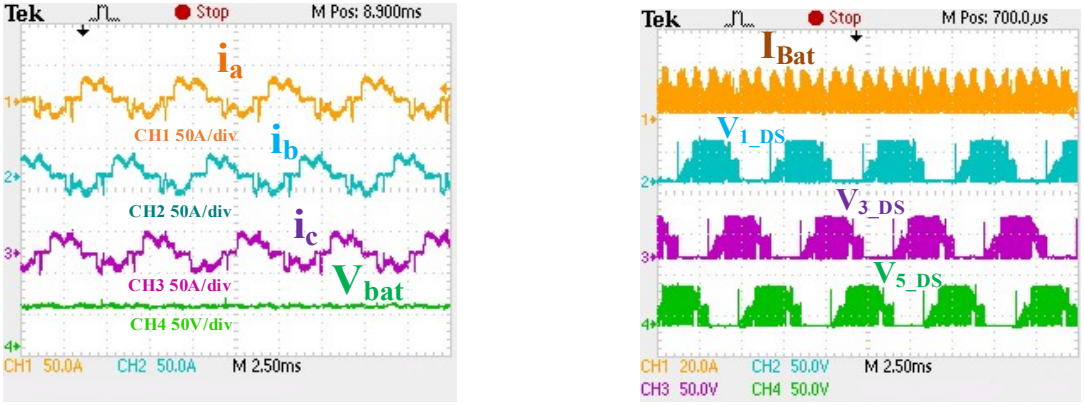

(a) (b)

Fig.4. 20 (a) represents motor line current i_a , i_b , i_c, with battery voltage (b) represents battery input current with voltage across the switch (V_{DS}).

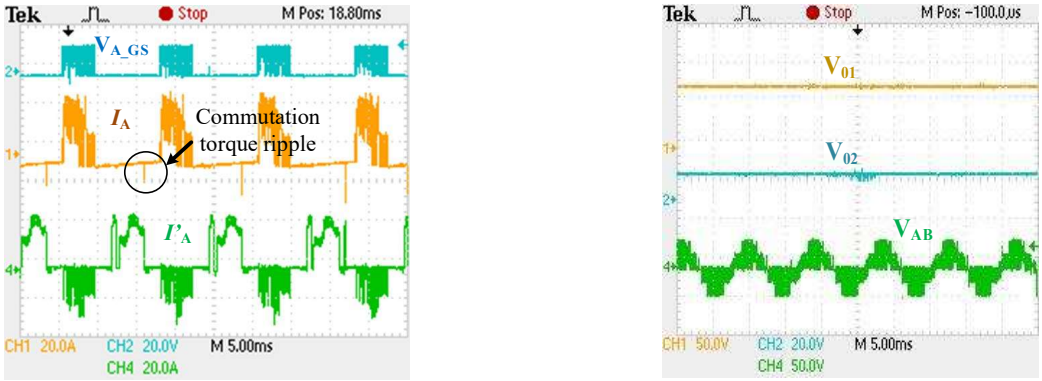

(a) (b)

Fig.4. 21 (a) Inverter switch current of one-leg when driven with High-PWM Low-ON switching scheme, (b) Multioutput with line voltage (V_{AB}) during motoring operation.

b) Commutation torque ripple elimination and auxiliary power supply during motoring operation:

The inverter phase -A, upper and lower leg switch current, with its switching, is represented in Fig.4. 21(a) by I_A, I'_A, and $V_{A\text{-}GS}$, respectively. The commutation current ripple from the lower switch current I'_A is greatly minimized. In a similar way, the commutation current ripple from the inverter lower switch currents I'_B and I'_C is also minimized.

Multioutput voltages during motoring operation are shown in Fig.4. 21(b). In this process, a 72 V (V_{01}) and 12 V (V_{02}) output are generated from a 48 V battery for the auxiliary power supply. The line voltage V_{AB} during the motoring operation is also shown in that one.

c) Voltage regulation of motoring mode during load dynamic

The operation of the proposed converter in motoring mode is analyzed by applying load dynamics in high-power and low-power auxiliaries, as shown in Fig.4. 22. Fig.4. 22(a) illustrates the behavior of the high-power auxiliary voltage, low-power auxiliary voltage, inverter line voltages (V_{01}, V_{02}, V_{AB}), and the high-power auxiliary load current (I_{01}) during the application of a dynamic load to the high-power auxiliary system. Further, a load dynamic applied to the low-power auxiliary and the converter response is shown in Fig.4. 22(b). where V_{bat}, V_{01}, V_{02}, and I_{02} represent the battery voltage, high-power auxiliary voltage, low-power auxiliary voltage, and current, respectively.

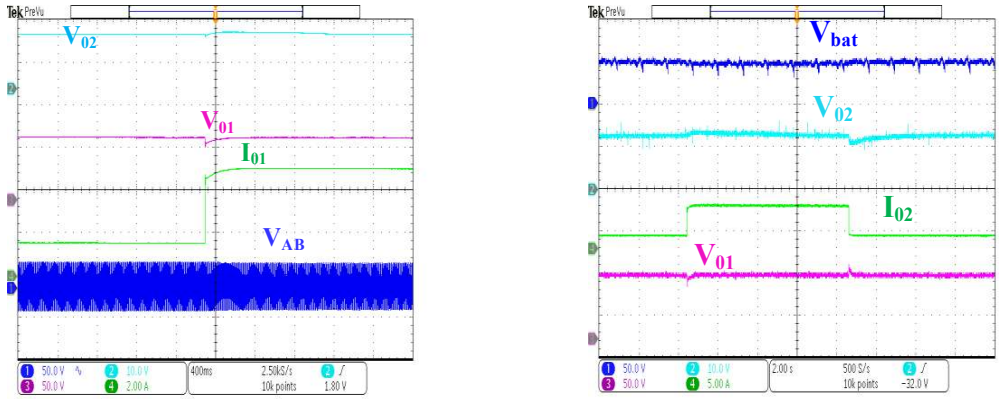

(a) (b)

Fig.4. 22 Load dynamic during motoring mode, (a) Load dynamic at high-power auxiliaries, and (b) Load dynamic at the low-power auxiliaries.

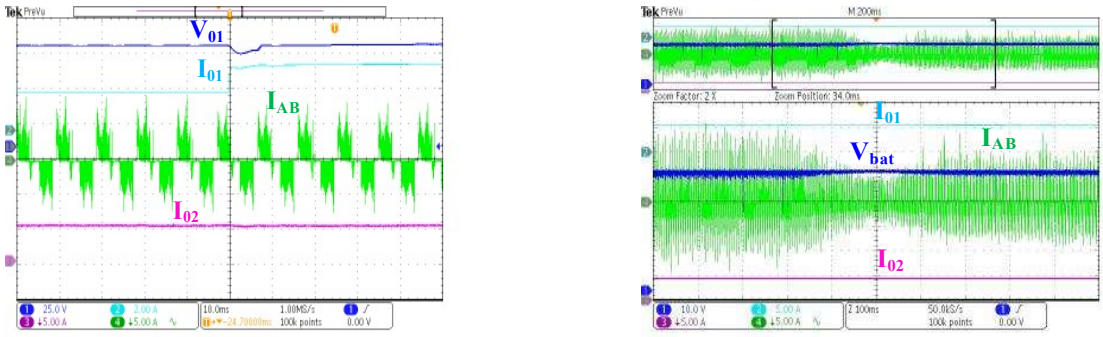

(a) (b)

Fig.4. 23 Dynamic result of the proposed converter during motoring mode(a) load dynamics in high-power auxiliaries, and (b) change in the speed of the motor.

The BLDC motor and auxiliary loads are connected in parallel, and their operations are independent of each other. If the auxiliary power varies, then that power is not reflected in the motor operation, as shown in Fig.4. 23(a). Further, the speed variation is applied to the BLDC

motor, and it does not reflect any current variation of the low-power and the high-power auxiliaries of the cabin, as shown in Fig.4. 23(b).

4.7.1.3 V2V charging operation with the auxiliary power supply

In multimode operation, the proposed power converters from both vehicles are connected to facilitate battery charging through a V2V connection. The boost multi-output feature of the proposed converter is utilized for efficient V2V charging.

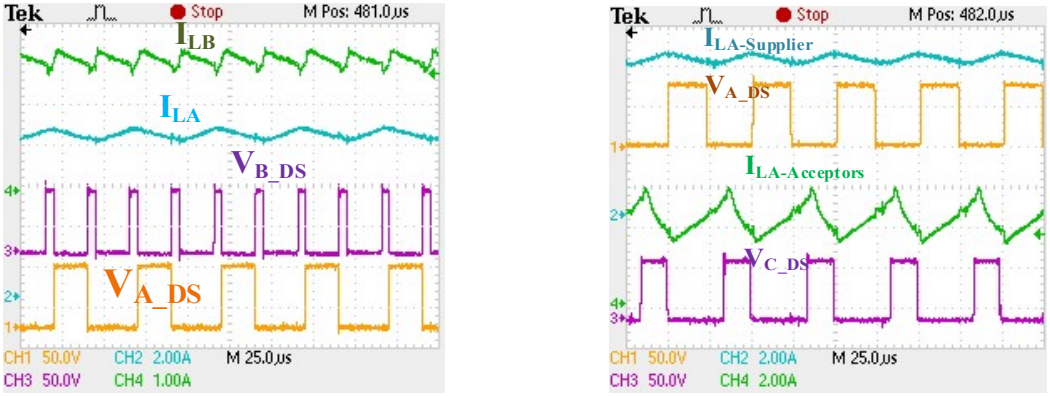

(a) (b)

Fig.4. 24 (a) The inductors L_A and L_B flux balance with respect to drain to source voltage of switch S_A, and S_B, during multioutput and (b) S_A, S_C switching voltages $V_{A\text{-}DS}$, $V_{C\text{-}DS}$, and according to them, the inductor L_A's currents $I_{LA\text{-}Supplier}$, $I_{LA\text{-}Acceptor}$, charging.

a) Multioutput operation of the proposed converter

The proposed converter switching operation during multioutput operation is shown in Fig.4. 24(a). where I_{LA} and I_{LB} represent the current profile of the inductors L_A, and L_B, and $V_{A\text{-}DS}$ and $V_{B\text{-}DS}$ represent the load voltage across the switch S_A and S_B.

b) V2V charging operation

During the V2V charging operation, the current profile of inductor L_A of the energy supplier EV, with switch voltage V_{A_CD} across the switch S_A, and the current profile of inductor L_A of the energy acceptor EV, with switch voltage V_{C_DS} across the switch S_C are shown in Fig.4. 24(b).

c) Available output voltages during V2V charging

Available voltages during V2V charging operation are shown in Fig. 26(a). where V_{EV1}, V_{01}, and V_{02} represent the battery voltage, high-power and low-power auxiliary voltages of the energy supplier vehicle, and V_{EV2} represents the battery voltage of the energy acceptor.

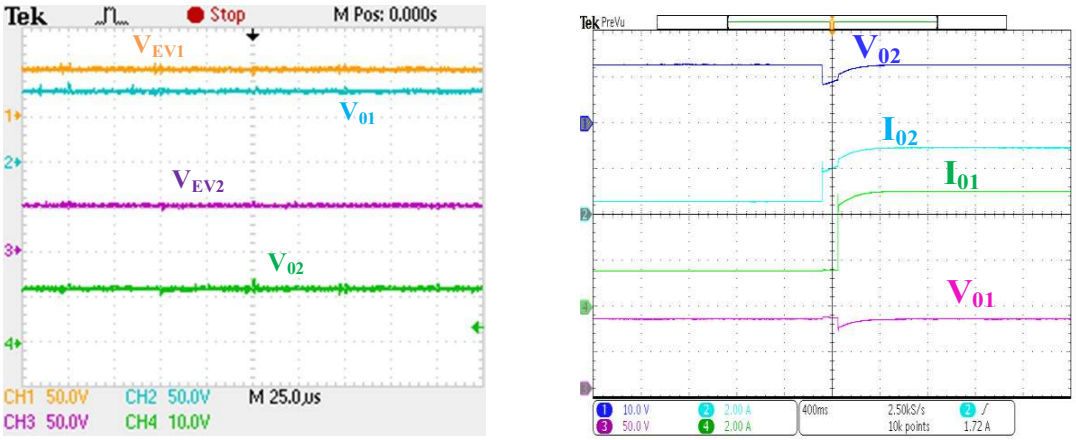

(a) (b)

Fig.4. 25 V2V operation of the proposed converter, (a) Available voltages during V2V charging, and (b) simultaneously applied the load dynamics in the low-power and high-power auxiliaries.

d) Load dynamic during V2V charging mode of operation

To verify the voltage regulation during V2V operation, a simultaneous load is applied at the low-power and high-power auxiliaries, as shown in Fig.4. 25. The V_{01} and V_{02} represent the set auxiliaries' voltages, and I_{01} and I_{02} represent the corresponding load current during V2V charging.

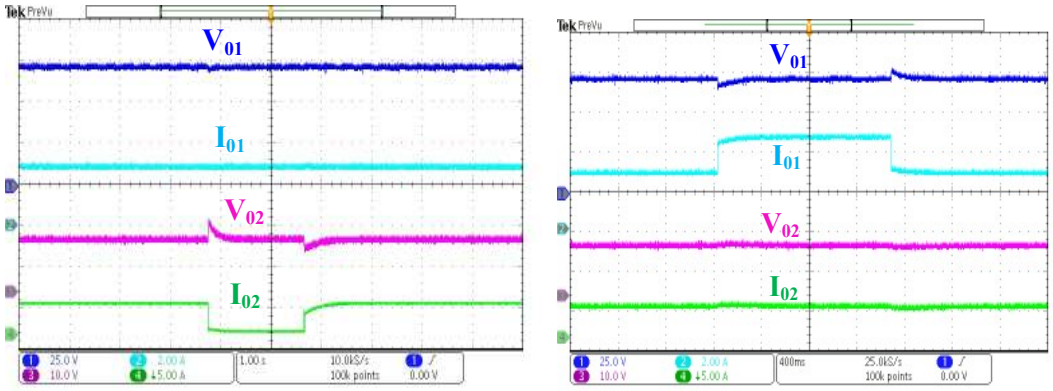

(a) (b)

Fig.4. 26 Current sharing between 72 V and 12 V during different load conditions, (a) current sharing of high-power auxiliaries unaffected by variation in a load of low-power auxiliaries, (b)current sharing of low-power auxiliaries unaffected by variation in a load of high-power auxiliaries.

Both 72 V and 12 V loads are connected in parallel and made independent of each other with the help of a control scheme. If the load is applied to the low-power auxiliary voltage (12 V), then there is no influence of the load connected to the high-power auxiliary voltage (72V),

as shown in Fig.4. 26(a). Further, if the load change is applied at the 72 V terminal, then there is no impact on the 12 V auxiliary supply, as shown in Fig.4. 26(b). Further, according to the battery chemistry, the rate of charge is adjusted with the help of the controller.

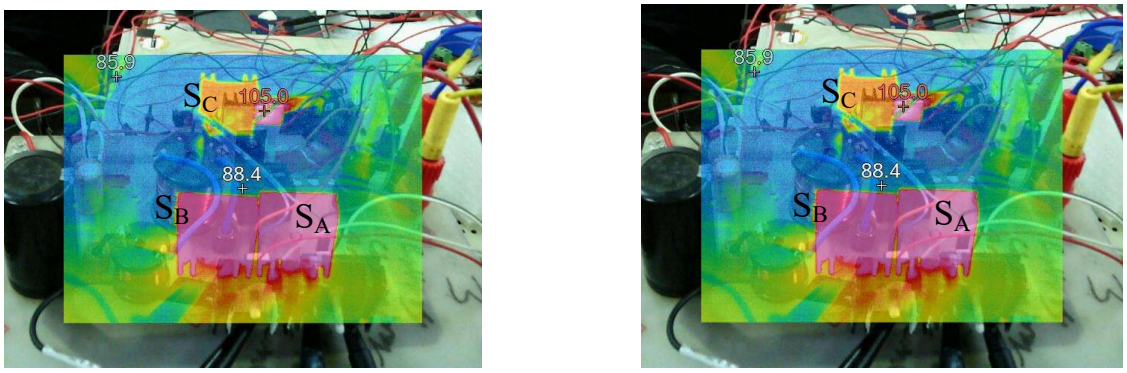

(a) (b)

Fig.4. 27 Thermal image of the proposed converter, (a) starting of the converter, and (b) after half an hour of the converter's operation.

4.7.2 Thermal profile of the proposed power converter

In all modes of operation, the switching area has been identified as the primary hotspot in the converter. This finding is validated by the thermal image analysis of the proposed converter, as shown in Fig.4. 27. These thermal images are taken in two stages of the converter: 1) in the initial stage after just starting the operation of the converter, as shown in Fig.4. 27(a). The main hot spot of the converter is the switches, whose temperature is 105^0 F (40^0 C). After 30 minutes, this temperature increases by 159^0 F (70^0 C), as shown in Fig.4. 27(b).

4.8 Conclusion

This chapter proposes On-board power processor having inherent V2V operation with reduced components. The proposed single converter serves for single-phase on-board charging, multioutput for the auxiliaries, motoring operation, and vehicle-to-vehicle (V2V) charging operation. The proposed converter uses 14 switches, which is a smaller number of switches with respect to the number of functions compared with similar prior converters. The multioutput features of the proposed converter are utilized for functionalities of V2V charging and auxiliary supplies, along with motoring and single-phase charging. Only six active switches from both of the vehicles are used for the V2V charging. In multioutput, the 12 V regulated output eliminates the additional demand for the 12 V battery and its charger. Further, the 72 V regulated output decreases the current requirement to feed the high-power auxiliaries.

The converter's efficiency in single-phase on-board charging, motoring operation, and V2V charging modes is 91.88 %, 92.3 %, and 93%, respectively, nearly 90 % of its rated load. Further, the thermal stability of the proposed converter is added in the experimental section. A laboratory-scale prototype is developed, which tests 780 W in charging mode, 1000 W in motoring mode, and 480 W during V2V changing operation.

The work carried out in this chapter has some limitations: 1) The proposed power processor cannot provide the vehicle-to-grid power supply. 2) However, with the growing penetration of electric vehicles, the load profile of the power grid has become increasingly dynamic, resulting in fluctuations in baseline electricity demand [116].

The next chapter introduces new opportunities for electricity trading through the integration of vehicle-to-grid (V2G) technology [117], [118], [119], [120], [121], [122], [123]. To enable V2G capability, the proposed power processor architecture is modified to support bidirectional power flow without increasing the number of switches. This is accomplished by replacing the diodes D1 and D2 in the original converter (as presented in Chapter 4) with controllable switches, allowing seamless V2G operation within the same hardware framework.